

Critical Reinvestigation on Vibronic Couplings in Picene from View of Vibronic Coupling Density Analysis

Tohru Sato,* Naoya Iwahara, and Kazuyoshi Tanaka

*Department of Molecular Engineering, Graduate School of Engineering,
Kyoto University, Kyoto 615-8510, Japan*

(Dated: October 29, 2018)

Abstract

Vibronic coupling constants in the monoanionic, trianionic, and excited states of picene are evaluated from the total energy gradients using the density functional theory. Employing the calculated vibronic coupling constants in the excited state of the neutral molecule, electron energy loss spectrum (EELS) is simulated to be compared with the experimental spectrum. The calculated vibronic coupling constants are analyzed in terms of the vibronic coupling density which enables us to analyze vibronic couplings based on the relation between the electronic and vibrational structures. The vibronic coupling constants reported by Kato *et al.* [*J. Chem. Phys.* **116**, 3420(2002) and *Phys. Rev. Lett.* **107**, 077001 (2011)] are critically discussed based on the vibronic coupling density analysis.

PACS numbers: 71.38.-k,79.20.Uv,33.20.Wr

After the discovery of the superconductivity in alkali-metal (K, Rb) doped picene,¹ experimental and theoretical studies on the electronic structure on the picene have been piled up.²⁻¹⁴ The vibronic coupling (electron-vibration coupling)¹⁵ is an important interaction in the electronic properties such as superconductivity. Okazaki *et al.* have discussed an importance of the vibronic couplings in doped picene based on their photoelectron spectra (PES).² Therefore, evaluation of the vibronic coupling constants (VCC) is crucial to discuss electronic properties of doped picenes. Some authors have published the VCCs of picene anions.^{10,11,16,17} However, some of the calculated VCCs are controversial. Subedi and Boeri have concluded that the electron-phonon coupling of the modes around 1600 cm⁻¹ are strong,¹⁰ while those calculated by Kato *et al* are weak in this region.^{11,16,17}

Vibronic effects can be experimentally observed in spectra.¹⁵ Roth *et al.* measured electron energy loss spectrum (EELS) of pristine picene at 20 K.⁵ They have observed vibronic progressions in the EELS of the intramolecular excitation to $S_2(^1B_2)$ state.

We have recently published calculation of the VCCs in C_{60}^- from the gradients of the total energies.¹⁸ The results are consistent with the experimental observation of the PES by Wang *et al.*¹⁹ We have proposed a concept, *vibronic coupling density* (VCD).^{20,21} Based on the VCD, we can discuss vibronic couplings from view of electronic and vibrational structures. On the basis of the VCD analysis, we have succeeded in designing carrier-transporting molecules with small vibronic couplings which is required in organic electronics such as organic light-emitting diodes (OLED).^{22,23}

In this work, we report the VCCs of the excited state of the free molecule in the neutral state, the monoanionic, and the trianionic states of the free molecule based on the same method of calculation employed in the calculation for C_{60}^- . Using the VCCs of the excited 1B_2 state, we simulate EELS and compare the spectrum with the experimental one.⁵ From the view of the VCD analysis, we critically discuss the previous VCCs in Refs. 11, 16, and 17.

We evaluated VCCs of mode α V_α from the gradients of the adiabatic potential energy surface E with respect to a mass-weighted normal coordinates Q_α :^{18,22-24}

$$V_\alpha = \left\langle \Psi \left| \left(\frac{\partial \hat{H}}{\partial Q_\alpha} \right)_{\mathbf{R}_0} \right| \Psi \right\rangle = \left(\frac{\partial E}{\partial Q_\alpha} \right)_{\mathbf{R}_0}, \quad (1)$$

where \hat{H} denotes a molecular Hamiltonian, \mathbf{R}_0 is the equilibrium geometry of the ground state of the neutral picene, Ψ is an electronic wavefunction of the excited or anionic state at

\mathbf{R}_0 , and the phase of a normal mode α is chosen so that V_α becomes negative. The vibronic Hamiltonian is written as

$$\hat{H}_{\text{vibro}} = \sum_{\alpha} \left[\hat{T}(Q_{\alpha}) + \frac{1}{2} \omega_{\alpha}^2 Q_{\alpha}^2 + V_{\alpha} Q_{\alpha} \right], \quad (2)$$

where $\hat{T}(Q_{\alpha})$ denotes kinetic energy operator of a vibration and ω_{α} vibrational frequency. We employed Becke’s hybrid functional (B3LYP)²⁵ and Perdew and Wang’s one with generalized gradient approximation (PW91)²⁶ with the triple-zeta 6-311+G(d,p) basis set. The geometries were optimized for the neutral ground state. The optimized structures with C_{2v} symmetry were checked with vibrational analysis to be a minimum. The time-dependent density-functional-theory is applied for the excited state calculations. We performed analytical force-calculations for the excited and the anionic states to obtain the VCCs.²⁷ The electronic and vibrational structures as well as the forces were obtained using a program package, Gaussian 09.²⁷ The VCCs are calculated using our codes.

Since the fine structure observed in the EELS by Roth *et al.*⁵ can originate from the vibronic couplings which they did not take into account in Ref. 3, we simulated the EELS to find an appropriate functional for the VCC calculations. EELS was simulated employing the same method as described in Ref. 18. We considered thermal excitation at 20K where Roth *et al.* observed the EELS. The calculated excitation energies are 3.7040 and 3.2520 eV for the B3LYP and PW91 functionals, respectively. The result using the PW91 functional reproduces well the experimental excitation energy 3.25 eV. Using the calculated VCCs in the $S_2(^1B_2)$ state, we simulated the EELS (FIGs. 1). In the simulations, the 0-0 transition is set to 3.24 eV, and the linewidth σ is assumed to be 270 cm^{-1} (The FWHM is 39.4 meV). The calculated VCCs²⁸ as well as the vibrational frequencies are tabulated in Supporting Information. The spectrum calculated employing the PW91 functional (FIG. 1(a)) shows a better fit than that using the B3LYP functional (FIG. 1(b)). In the calculation employing the B3LYP, the second strongest vibronic couplings around 1350 cm^{-1} are estimated larger than those in the result using the PW91.²⁹ Therefore, the relative intensities of EELS in the lower energy are reproduced employing the PW91.³⁰ Judging from the calculations of the excitation energies and the simulated spectra, we employ the PW91 functional hereafter for the calculation of the ionic states. The further comparisons of functionals are out of the scope in the present work.

We calculated the VCCs V_{α} in the monoanion (2A_2), dianion (1A_1), and trianion (2B_1)

(a) PW91

(b) B3LYP

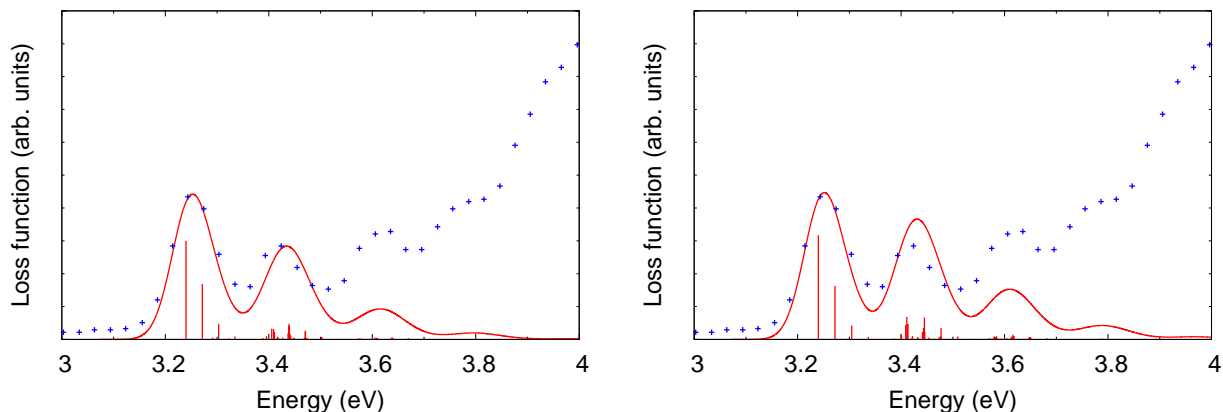


FIG. 1. (Color online) Red lines are simulated electron energy loss spectra (EELS) calculated by (a) the PW91 and (b) the B3LYP functional. Blue dots indicate the experimental one by Roth *et al.*⁵ The 0-0 transition is set to 3.24 eV. The other parameters employed in the simulations are $T = 20$ K and $\sigma = 270$ cm^{-1} .

(see Supporting Information). Kato *et al.* have calculated orbital vibronic coupling constants (OVCC) of the lowest unoccupied molecular orbitals (LUMO) and next LUMO (NLUMO).^{11,16,17} Hence we also calculated the OVCCs $V_{i,\alpha}$ from the VCCs V_α for comparison with the ones previously reported. The vibronic Hamiltonian (2) is mapped onto a model Hamiltonian. The model Hamiltonian considered in Refs. 10 and 11 is written as follows:

$$\hat{H}_{\text{vibro}} = \sum_{\alpha,i,\sigma} \hbar\omega_\alpha \left[\hat{b}_\alpha^\dagger \hat{b}_\alpha + \frac{g_{i,\alpha}}{\sqrt{2}} (\hat{b}_\alpha^\dagger + \hat{b}_\alpha) \hat{c}_{i\sigma}^\dagger \hat{c}_{i\sigma} \right], \quad (3)$$

where orbitals i are LUMO (L) and NLUMO (NL), and α runs over all the active a_1 modes.²⁸ The dimensionless OVCC $g_{i,\alpha}$ is defined by $g_{i,\alpha} = V_{i,\alpha} / \sqrt{\hbar\omega_\alpha^3}$. $\hat{c}_{i\sigma}^\dagger$ ($\hat{c}_{i\sigma}$) is the creation (annihilation) operator of orbital i and spin σ , and \hat{b}_α^\dagger (\hat{b}_α) is the creation (annihilation) operator of mode α . The OVCCs of LUMO $V_{L,\alpha}$ and NLUMO $V_{NL,\alpha}$ are obtained from the VCCs of monoanion $V_{\text{mono},\alpha}$ and the difference between VCCs of trianion $V_{\text{tri},\alpha}$ and dianion $V_{\text{di},\alpha}$, respectively: $V_{L,\alpha} = V_{\text{mono},\alpha}$ and $V_{NL,\alpha} = V_{\text{tri},\alpha} - V_{\text{di},\alpha}$. It should be noted that the present OVCCs effectively incorporate the contributions from all the occupied orbitals which are important in quantitative arguments.¹⁸ The OVCCs $V_{i,\alpha}$ and intramolecular electron-phonon couplings $\lambda_{i,\alpha}/N(0) = V_{i,\alpha}^2/\omega_\alpha^2$ are shown in FIGs. 2 and tabulated in Supporting Informa-

(a) Monoanion

(b) Trianion

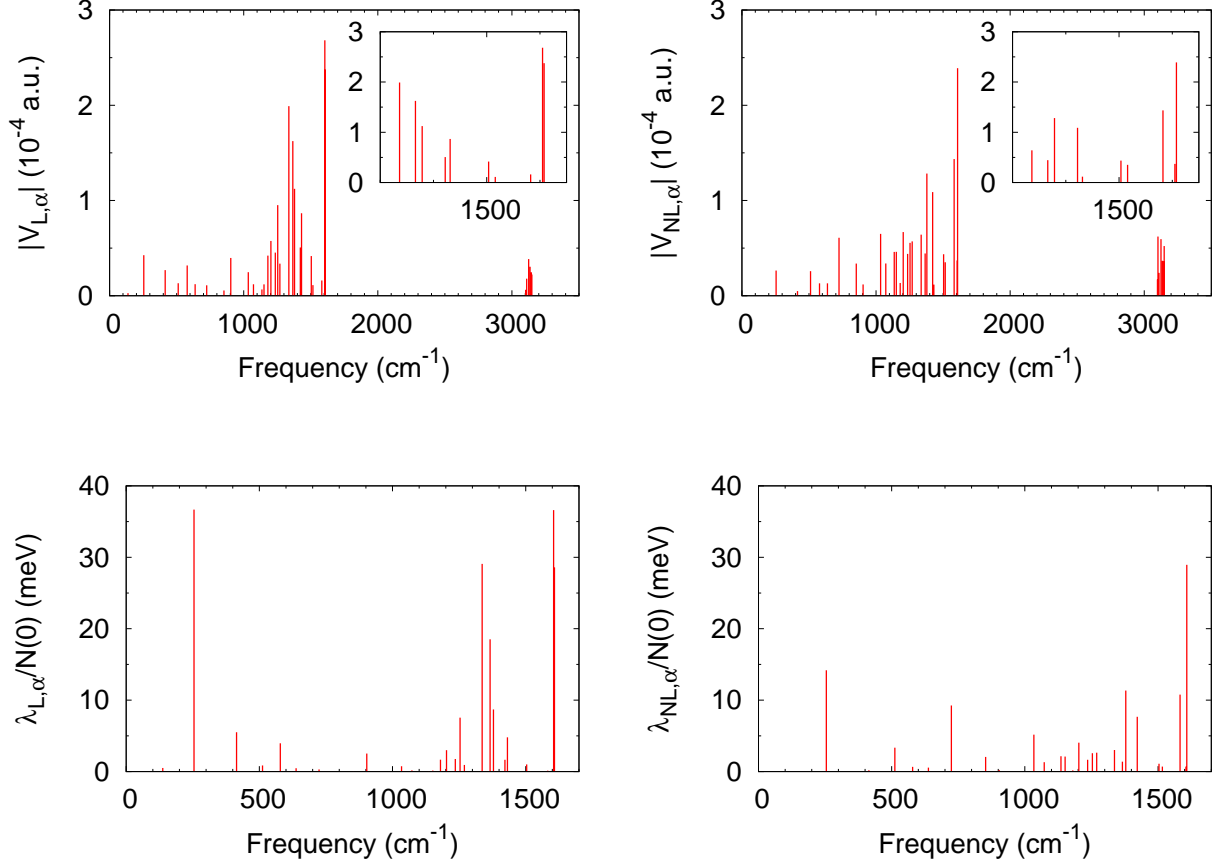


FIG. 2. (Color online) Calculated (top) orbital vibronic coupling constants $V_{i,\alpha}$ and (bottom) electron-phonon couplings $\lambda_{i,\alpha}/N(0)$ in the (a) monoanion and the (b) trianion. The subscripts L and NL denote LUMO and NLUMO, respectively. Insets show the orbital vibronic couplings between 1300 to 1650 cm^{-1} .

tion. $N(0)$ is the density of states at the Fermi level.

In both the monoanion and trianion, two sets of modes with strong VCCs are observed: (1) the maximal coupling modes around 1600 cm^{-1} and (2) the second group of strong modes around 1350 cm^{-1} . This is qualitatively consistent with the calculations by Subedi and Boeri.^{10,31} However, in the calculations of Refs. 11, 16, and 17,³² the modes around 1600 cm^{-1} are weak for both the monoanion and trianion. The total electron-phonon couplings $\lambda_L/N(0) = \sum_{\alpha} \lambda_{L,\alpha}/N(0)$ and $\lambda_{NL}/N(0) = \sum_{\alpha} \lambda_{NL,\alpha}/N(0)$ are 196.6 meV and 119.9 meV, respectively. The total coupling of the trianion $\lambda_{NL}/N(0)$ is in line with that of Subedi

and Boeri (110 ± 5 meV).¹⁰ On the other hand, in Ref. 11, $\lambda_L/N(0) = 178$ meV and $\lambda_{NL}/N(0) = 206$ meV. They underestimated and overestimated the total couplings for the monoanion and trianion, respectively.

We will discuss the disagreement from view of the electronic and vibrational structures. The calculated VCCs can be rationalized based on the vibronic coupling density.^{20,21} A VCD η_α is defined as

$$\eta_\alpha(\mathbf{r}) = \Delta\rho(\mathbf{r}) \times v_\alpha(\mathbf{r}), \quad (4)$$

where $\Delta\rho(\mathbf{r}) = \rho(\mathbf{r}) - \rho_0(\mathbf{r})$ is the electron density difference between the electron density of an ionic state ρ and that of a neutral state ρ_0 . The potential derivative $v_\alpha(\mathbf{r})$ is the derivative with respect to a mass-weighted normal coordinate Q_α of the potential $u(\mathbf{r})$ acting on one electron at a position \mathbf{r} from all the nuclei. The vibronic coupling constant is equal to the integral of $\eta_\alpha(\mathbf{r})$ over space \mathbf{r} :

$$V_\alpha = \int d^3\mathbf{r} \eta_\alpha(\mathbf{r}). \quad (5)$$

The VCD gives a local picture of the vibronic coupling, and hence enables us to discuss the strength of the coupling qualitatively.

We will concentrate on the $a_1(27)$ mode of the maximal-coupling mode around 1600 cm^{-1} and the $a_1(21)$ mode from the second group around 1350 cm^{-1} because the $a_1(27)$ and $a_1(21)$ modes are close to the mode 5 in Ref. 10 and the 21st mode (ν_{21}) in Ref. 11, respectively. FIGs. 3 show the potential derivatives $v_\alpha(\mathbf{r})$ for the $a_1(27)$ and the $a_1(21)$ modes. The distribution of the potential derivative with respect to the $a_1(27)$ mode is located on the armchair-edges of the central three hexagons. On the other hand, that with respect to the $a_1(21)$ mode is on the terminal hexagons.

FIG. 4(b) shows the electron density difference $\Delta\rho$ of the monoanion. Since an additional electron occupies the LUMO (FIG. 4(a)), the positive π density (white) appears in $\Delta\rho$. It should be noted that there occurs decrease of the σ density (blue) in the molecular plane. Such a polarized density originates from the Coulomb interactions between the electron occupying the LUMO and all electrons in doubly occupied orbitals below the highest occupied molecular orbital (HOMO).²⁰

FIGs. 5 show the vibronic coupling densities $\eta_\alpha(\mathbf{r})$ of the monoanion with respect to the $a_1(27)$ and $a_1(21)$ modes. As for the $a_1(27)$, the electron density difference $\Delta\rho(\mathbf{r})$ shows considerable overlap with the potential derivative $v_\alpha(\mathbf{r})$. On the other hand, $\Delta\rho(\mathbf{r})$ does not

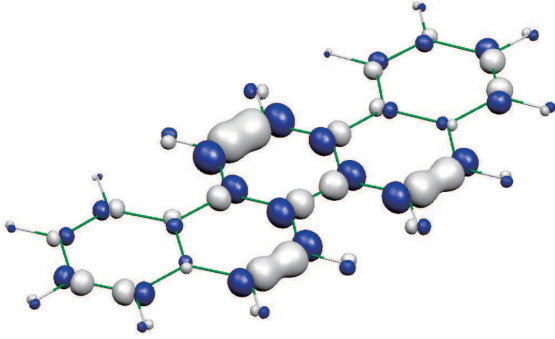
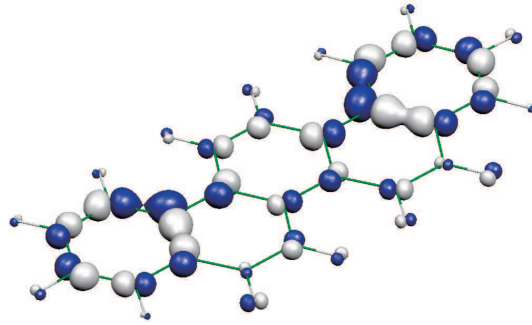
(a) $a_1(27)$ (1605 cm^{-1})(b) $a_1(21)$ (1379 cm^{-1})

FIG. 3. (Color online) Potential derivatives v_α for (a) $a_1(27)$ (1605 cm^{-1}) and (b) $a_1(21)$ (1379 cm^{-1}) modes. White and blue areas indicate positive and negative, respectively. The threshold is 1.0×10^{-2} a.u.

(a) LUMO

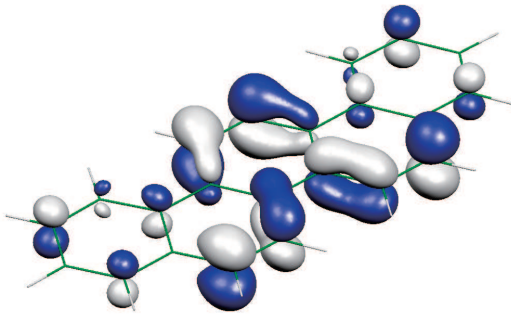
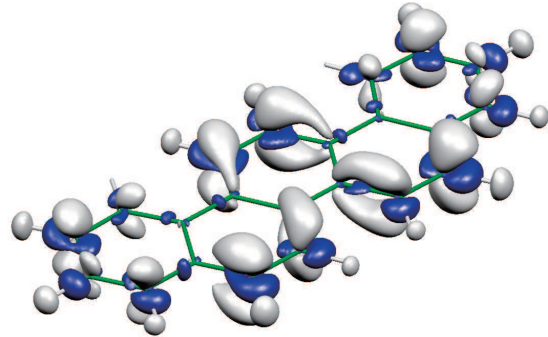
(b) $\Delta\rho$ 

FIG. 4. (Color online) (a) LUMO and (b) electron density difference $\Delta\rho$ for the monoanion. White and blue areas indicate positive and negative, respectively. The threshold is 5.0×10^{-2} a.u. for LUMO and 1.8×10^{-3} a.u. for $\Delta\rho$.

significantly overlap $v_\alpha(\mathbf{r})$ for the $a_1(21)$ mode. Therefore, the VCD η_α (4) for the $a_1(27)$ is larger than that for the $a_1(21)$. Particularly, η_α for the $a_1(27)$ has the large distribution on the central three armchair-edges. Accordingly, the VCC of the $a_1(27)$ mode is larger than that of the $a_1(21)$ mode.

The VCD η_α for the $a_1(27)$ mode on the bonds appears due to the polarization of $\Delta\rho$, thus neglecting such a polarization can give rise to quantitative, or sometimes qualitative, errors in VCC calculations based on the orbital levels.¹⁸ In addition, an electron density difference is usually different from the orbital density of HOMO or LUMO. Many-body effect sometimes

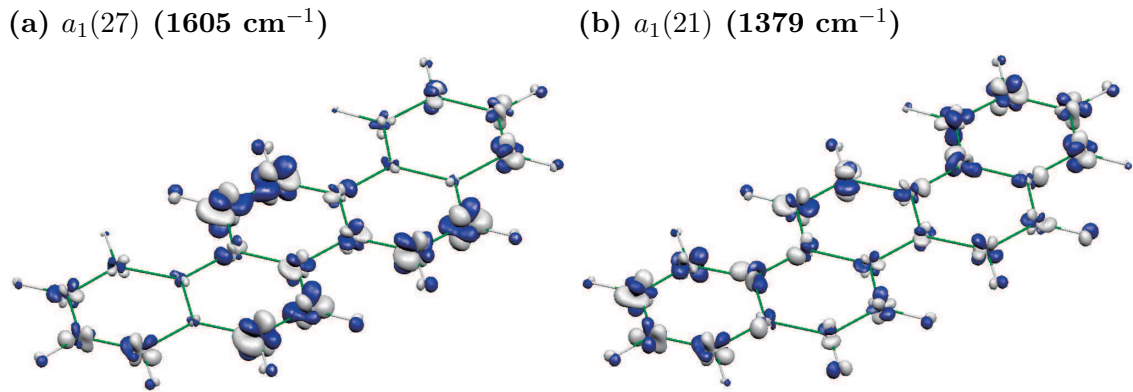


FIG. 5. (Color online) Vibronic coupling densities for (a) $a_1(27)$ (1605 cm^{-1}) and (b) $a_1(21)$ (1379 cm^{-1}) modes of the monoanion. White and blue areas indicate positive and negative, respectively. The threshold is 2.0×10^{-5} a.u.

TABLE I. Calculated frequencies (cm^{-1}) and orbital gradients $\partial\epsilon/\partial Q$ and total-energy gradients $\partial E/\partial Q$ as vibronic coupling constants (10^{-4} a.u.) for the selected modes of the monoanion. The subscripts L and S denote the neutral LUMO and the SOMO of the anion, respectively.

	Freq.	$\partial\epsilon_L/\partial Q$	$\partial\epsilon_S/\partial Q$	$\partial E/\partial Q$	
				Num.	Anal.
$a_1(2)$	254.5	0.372	0.475	0.426	0.426
$a_1(19)$	1336.4	2.019	1.889	1.988	1.990
$a_1(20)$	1366.1	1.872	1.365	1.639	1.624
$a_1(21)$	1378.8	0.820	1.335	1.130	1.123
$a_1(27)$	1604.9	3.070	2.281	2.706	2.682
$a_1(28)$	1607.9	2.090	2.580	2.377	2.374

plays a crucial role on the electron density difference, and therefore vibronic couplings.²⁴

Kato *et al.* have calculated VCCs as the gradients of the orbital levels (orbital gradients) with respect to normal coordinates.¹⁶ We also obtained the orbital gradients of selected modes from the neutral LUMO $\partial\epsilon_L/\partial Q_\alpha$ and from the singly occupied molecular orbital (SOMO) of the monoanion $\partial\epsilon_S/\partial Q_\alpha$ to compare the present VCCs calculated analytically from the total energy gradient as well as numerical gradients. The orbital gradients and

the numerical energy gradients were obtained by fitting linear and quadratic polynomials, respectively, in the range from -0.2 to 0.2 a.m.u.^{1/2} a_0 with a step size 0.05 a.m.u.^{1/2} a_0 where a_0 is the Bohr radius. These range and step size could be different from those of Kato *et al.* We summarize the results of the calculations in TABLE I. All the results indicate that the vibrational modes around 1600 cm⁻¹ have the maximal coupling.

Though the gradients of the LUMO level can yield results which are qualitatively consistent with the gradients of the total energy, the results in Refs. 11 and 16 are not the case. In their calculations, the vibrational mode around 1380 cm⁻¹ has the maximal coupling, 2.3×10^{-4} a.u. for the monoanion.¹⁶ However, since $\Delta\rho$ (see FIG.4(b)) is mainly located on the armchair-edges of the central three hexagons, it does not overlap with the potential derivatives v_α of the mode (FIG.3(b)), the VCC of the mode cannot be the maximal. Similar discussion holds for the mode around 1520 cm⁻¹ which has the maximal coupling, 2.6×10^{-4} a.u. for the trianion.¹¹

In summary, we calculated the VCCs of picene for the excited state 1B_2 of the neutral molecule, the monoanionic, and the trianionic states of the molecule from the gradients of the total energies with respect to the normal modes. In the previous studies, the VCCs calculated from the gradients of the orbital energies of the frontier level, LUMO. In other words, they have regarded the OVCCs of the LUMO as the VCCs. The present approach can provide quantitatively reliable VCCs, since all the occupied orbitals can contribute to the VCCs due to the selection rule. This has been discussed in Ref. 18 in detail. We simulated the EELS and compared the spectra with experimental spectrum by Roth *et al.* No comparison with experiments has been reported on the vibronic couplings in picene. Needless to say, such a comparison between the theoretical and the experimental results is necessary to obtain reliable VCCs. From these simulations, we determined an appropriate functional for the calculation of the vibronic couplings in picene. Using the functional which reproduces the EELS, we evaluated the vibronic coupling constants of the picene anions. The calculated vibronic couplings of the anions can be employed for assignments of spectra, for example, photoelectron spectra of the anions. We discussed the vibronic couplings of the picene anions in terms of the vibronic coupling density. Based on the analysis, the present vibronic couplings are reasonable compared with the values reported previously.

Numerical calculations were performed partly in the Supercomputer Laboratory of Kyoto University and Research Center for Computational Science, Okazaki, Japan. This work

was supported in part by the Japan Society for the Promotion of Science (JSPS) through its Funding Program for the Global COE Program “International Center for Integrated Research and Advanced Education in Materials Science” (No. B-09) of the Ministry of Education, Culture, Sports, Science and Technology (MEXT) of Japan.

* tsato@moleng.kyoto-u.ac.jp

- ¹ R. Mitsuhashi *et al.*, Nature **464**, 76 (2010).
- ² H. Okazaki *et al.*, Phys. Rev. B **82**, 195114 (2010).
- ³ F. Roth, M. Gatti, P. Cudazzo, M. Grobosch, B. Mahns, B. Büchner, A. Rubio, and M. Knupfer, New. J. Phys. **12**, 103036 (2010).
- ⁴ F. Roth, B. Mahns, B. Büchner, and M. Knupfer, Phys. Rev. B **83**, 144501 (2011).
- ⁵ F. Roth, B. Mahns, B. Büchner, and M. Knupfer, Phys. Rev. B **83**, 165436 (2011).
- ⁶ T. Kosugi, T. Miyake, S. Ishibashi, R. Arita, and H. Aoki, J. Phys. Soc. Jpn. **78**, 113704 (2009).
- ⁷ G. Giovannetti and M. Capone, Phys. Rev. B **83**, 134508 (2011).
- ⁸ M. Kim, B. I. Min, G. Lee, H. J. Kwon, Y. M. Rhee, and J. H. Shim, Phys. Rev. B **83**, 214510 (2011).
- ⁹ P. L. de Andres, A. Guijarro, and J. A. Vergés, Phys. Rev. B **83**, 245113 (2011).
- ¹⁰ A. Subedi and L. Boeri, Phys. Rev. B **84**, 020508(R) (2011).
- ¹¹ T. Kato, T. Kambe, and Y. Kubozono, Phys. Rev. Lett. **107**, 077001 (2011).
- ¹² M. Casula, M. Calandra, G. Profeta, and F. Mauri, Phys. Rev. Lett. **107**, 137006 1 (2011).
- ¹³ Y. Kubozono *et al.*, Phys. Chem. Chem. Phys. **13**, 16476 (2011).
- ¹⁴ T. Kosugi, T. Miyake, S. Ishibashi, R. Arita, and H. Aoki, Phys. Rev. B **84**, 214506 (2011).
- ¹⁵ I. B. Bersuker and V. Z. Polinger, *Vibronic Interactions in Molecules and Crystals* (Springer-Verlag, Berlin and Heidelberg, 1989).
- ¹⁶ T. Kato, K. Yoshizawa, and K. Hirao, J. Chem. Phys. **116**, 3420 (2002).
- ¹⁷ T. Kato and K. Hirao, in *Advances in Quantum Chemistry*, Vol. 44, edited by J. R. Sabin and E. Brändas (Elsevier Academic Press, San Diego, 2003) p. 257.
- ¹⁸ N. Iwahara, T. Sato, K. Tanaka, and L. F. Chibotaru, Phys. Rev. B **82**, 245409 (2010).
- ¹⁹ X. B. Wang, H. K. Woo, and L. S. Wang, J. Chem. Phys. **123**, 051106 (2005).
- ²⁰ T. Sato, K. Tokunaga, and K. Tanaka, J. Phys. Chem. A **112**, 758 (2008).

- ²¹ T. Sato, K. Tokunaga, N. Iwahara, K. Shizu, and K. Tanaka, in *The Jahn-Teller Effect: Fundamentals and Implications for Physics and Chemistry*, Springer Series in Chemical Physics, Vol. 97, edited by H. Köppel, D. R. Yarkony, and H. Barentzen (Springer-Verlag, Heidelberg Berlin, 2009) pp. 99–129.
- ²² K. Shizu, T. Sato, K. Tanaka, and H. Kaji, *Appl. Phys. Lett.* **97**, 142111 (2010).
- ²³ K. Shizu, T. Sato, A. Ito, K. Tanaka, and H. Kaji, *J. Mater. Chem.* **21**, 6375 (2011).
- ²⁴ T. Sato, K. Shizu, K. Uegaito, N. Iwahara, K. Tanaka, and H. Kaji, *Chem. Phys. Lett.* **507**, 151 (2011).
- ²⁵ A. D. Becke, *J. Chem. Phys.* **98**, 5648 (1993).
- ²⁶ J. P. Perdew, J. A. Chevary, S. H. Vosko, K. A. Jackson, M. R. Pederson, D. J. Singh, and C. Fiolhais, *Phys. Rev. B* **46**, 6671 (1992).
- ²⁷ M. J. Frisch *et al.*, *Gaussian 09, Revision B.01*, Wallingford CT (2010).
- ²⁸ From the selection rule for the vibronic coupling, the excited and anionic electronic states couple only to the a_1 modes.
- ²⁹ In terms of the electron-phonon couplings, the total coupling in the excited state obtained by the B3LYP (355.8 meV) is larger than that by the PW91 (291.4 meV) by 64 meV.
- ³⁰ The peaks in the higher energy than 3.6 eV include other excitations⁵, while we do not consider them in our simulation. Thus the simulated spectrum does not agree with experimental one in the energy range. Since we focus on S_2 , we do not consider the higher excitations.
- ³¹ Subedi and Boeri calculated the electron-phonon couplings using the density functional perturbation theory³³ within the local density approximation.
- ³² Kato *et al.* calculated the electron-phonon couplings from the gradients of orbital level using the B3LYP functional.
- ³³ S. Baroni, S. de Gironcoli, A. D. Corso, and P. Giannozzi, *Rev. Mod. Phys.* **73**, 515 (2001).